Steady two-layer flow in narrow channels of variable width

Roger E. Khayat and Guowen Tian
Department of Mechanical and Materials Engineering, The University of Western Ontario, London, Ontario, Canada N6A 5B9
(Received 24 May 2008; revised manuscript received 28 January 2009; published 30 April 2009)

The shape of the interface and pressure buildup for two-layered steady creeping flow inside a narrow channel of variable topography are examined in this study. The flow is assumed to be induced by the translation of the lower flat plate, similarly to lubrication flow. The interplay between channel topography and viscosity ratio, R_μ, is emphasized, in the absence of interfacial tension and gravity. For contracting channel and in the low R_μ range, the pressure increases everywhere in the channel monotonically with R_μ, reaching a maximum, and decreases as R_μ is increased further. In contrast, the interface level increases monotonically with R_μ. Channel modulation causes considerable pressure buildup. However, unlike the interface, which exhibits modulation, the pressure distribution along the channel remains qualitatively unaffected.

DOI: 10.1103/PhysRevE.79.046326 PACS number(s): 47.15.gm

I. INTRODUCTION

Interfacial multilayer flows have received much attention in the recent literature, for their importance in engineering processes, such as coating, polymer extrusion, oil transportation, as well as for their fundamental importance. Due to their industrial importance, many investigations have involved the mathematical modeling of these processes as well as studying the physical properties of the film as affected by various processing conditions. Interfaces between two adjacent fluids are susceptible to various kinds of hydrodynamic instabilities with different origins and diverse mechanisms of growth. In this study, the steady creeping two-layer flow inside a channel of variable geometry is examined.

A variety of two-layer flow configurations have been examined in the literature, the most common being gravity-driven flow of multilayered film on an inclined plane. [1] Charru and Hinch [2] obtained phase diagrams of interfacial instabilities in a two-layer Couette flow and suggested a mechanism for the long-wave instability. They established the critical level of flow conditions, namely, the flow rate or pressure gradient, for the onset of instability in the form of the fastest growing mode. They proposed a unified and more physical viewpoint of the instabilities that may arise in two-layer Couette flow. The instability of two-layer creeping flow in a channel with parallel-sided walls was examined by Pozrikidis [3]. A numerical calculation was performed for two-layer channel Stokes flow subject to two-dimensional perturbations, and the effect of the various geometrical and physical parameters on the flow was examined. Later Pozrikidis examined the gravity-driven creeping flow of two adjacent layers through a channel and down a plane wall. [4] The instability of two layers flowing through an inclined channel that is open at both ends was examined for creeping flow and in the absence of mean pressure gradient. Chen [5] concluded that the deformability of the free surface was a contributing factor in the growth of small perturbations and attributed the unstable behavior to resonance between the interface and free-surface waves. When the free surface is maintained flat by infinite surface tension, the instability does not appear.

Two-layer channel flows have been restricted to simple geometry, mainly the flow in a straight channel. Flow in variable channel geometry has, of course, been considered, but for single-phase flow. For creeping flow, the problem reduces to conventional lubrication flow. Most studies on hydrodynamic lubrication examined nominal point and line contact flows and concentrated on oil lubrication of Newtonian flow, [6,7] and non-Newtonian flow, such as those based on the Eyring [8,9] and the power law [10] models. Grease lubrication, which is based on relatively simple rheological models such as Bingham fluids, has also been examined. [11] The influence of inertia has also been assessed. The reader is referred to the study by Zhou *et al.* [12] and references therein for studies on the flow inside modulated channels, and to Siddique and Khayat [13] for more general flow configurations. More recently, Alba *et al.* [14] examined the interplay between inertia and interfacial tension for the free surface flow of two superposed fluids.

Despite the numerous studies devoted to two-layer flow, significant questions remain unanswered. In particular, the influence of the shape of channel on the interface and pressure has not been investigated. The interplay between viscosity ratio and channel topography is of fundamental and practical significance. In this paper, the behavior of two superposed thin layers of immiscible fluids flowing steadily through an arbitrary-sided walled narrow channel is examined in the absence of inertia. In particular, the influence of viscosity ratio, channel contraction, and modulation on the interface profile and pressure distribution will be emphasized.

II. PROBLEM FORMULATION AND SOLUTION PROCEDURE

In this section, the two-fluid film flow configuration is introduced, along with the prescribed governing equations and boundary conditions. The lubrication assumption is adopted for the formulation of the problem.

A. Governing equations and boundary conditions

Consider the steady two-layer lubrication flow of two incompressible Newtonian fluid layers of identical density in the (X,Y) plane. Let U, V, and P denote the velocity com-

ponents and pressure, respectively. The fluids are confined between two rigid boundaries, the lower boundary, $Y=0$, being straight and moving at a velocity U_0, and the upper boundary being stationary and of variable height, $Y=H(X)$. The bottom layer is layer 1 and the top layer is layer 2. The viscosity of layer 1 is μ_1 and that of layer 2 is μ_2. The fluids are assumed to enter the channel domain $[0,L]$ from an infinite fluid pool at $X=0$ where each layer thickness is assumed to be fixed. The interface height is given by $y=E(X)$. Thus, $E_0=E(0)$ is the thickness or height of layer 1 and $H_0=H(0)$ is the *total* thickness of both layers 1 and 2 or height of the upper boundary at $X=0$. In this case, the thickness of the top layer at $X=0$ is H_0-E_0. The two layers are assumed to exit freely (into a pool) at $X=L$. The flow domain is deliberately set to a finite length, which is typically the case of lubrication flows [15]. Similar flow configurations with finite domain are also encountered in manufacturing processes such as calendaring, fiber spinning, and film casting. [16] In this work, L and E_0 will be taken as the reference length and depth, respectively, and μ_1 will be the reference viscosity. Note that E_0 and H_0 are assumed to be of the same order of magnitude. For a thin film, $L \gg E_0$ or H_0. In this case, the aspect ratio $\varepsilon=E_0/L \ll 1$ and will be used as the small parameter in the problem.

Following the usual procedure in lubrication or thin-film flow theory, one introduces dimensionless coordinates, x and y, scaled by L and E_0, respectively, and the corresponding velocity components, u and v, scaled by U and E_0U/L, respectively. In this case, an adequate scale for the pressure, p, is $\varepsilon^{-2}\mu_1 UL^{-1}$. The nondimensional interface and upper boundary heights are denoted by $\eta(x)$ and $h(x)$, respectively. More explicitly, the dimensionless variables are given by

$$x=\frac{X}{L}, \quad y=\frac{Y}{E_0}, \quad u=\frac{U}{U_0}, \quad v=\frac{V}{\varepsilon U_0}, \quad p=\frac{\varepsilon^2 L}{\mu_1 U_0}P,$$

$$\eta=\frac{E}{E_0}, \quad h=\frac{H}{E_0}. \tag{1}$$

In the absence of gravity and interfacial tension effects, the similarity parameters for the problem are the aspect ratio, ε, viscosity ratio, R_μ, height ratio, R_H, and the Reynolds number, Re, which are introduced as

$$\varepsilon=\frac{E_0}{L}, \quad R_\mu=\frac{\mu_2}{\mu_1}, \quad R_H=\frac{H_0}{E_0}, \quad \mathrm{Re}=\frac{\rho U_0 L}{\mu_1}. \tag{2}$$

The effects of surface and interfacial tensions were examined recently for two-layer film flow by Alba *et al.* [14] Note R_H is the ratio of the thickness of the entire film to that of the lower layer at $x=0$, and $R_H>1$. The problem is examined in the (x,y) plane and is illustrated schematically in Fig. 1. Here $x\in[0,1]$. Recall that the lower plate remains straight and moves at a normalized unit speed. Upon casting the governing equations in dimensionless form, the continuity equation retains its original form in each layer to read

$$u_x+v_y=0, \tag{3}$$

and holds in layer 1 $(0\le y\le \eta)$ and layer 2 $(\eta\le y\le h)$. A subscript with respect to x or y denotes partial differentiation.

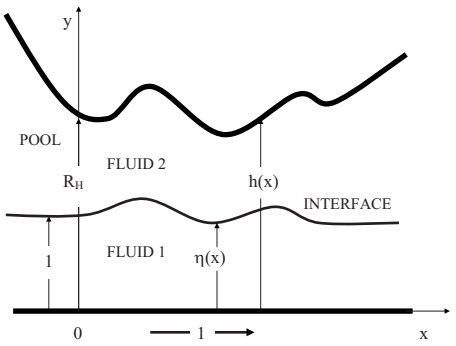

FIG. 1. Schematic illustration of the flow configuration for two-layer fluid and dimensionless notation used.

The conservation of linear momentum equation, on the other hand, is significantly simplified given the small thickness-to-length ratio $(\varepsilon \ll 1)$ for a thin layer. In this case, the viscous elongational terms are dropped for each layer. The y-momentum equation reduces to its hydrostatic part, which in turn suggests, for negligible gravity and interfacial tension, that the pressure simply remains constant across the channel, but varies streamwise. In this case, the streamwise momentum equation in layers 1 and 2 takes the respective form

$$\varepsilon^2\,\mathrm{Re}(uu_x+vu_y)=-\frac{dp}{dx}+u_{yy}, \quad 0\le y\le \eta, \tag{4a}$$

$$\varepsilon^2\,\mathrm{Re}(uu_x+vu_y)=-\frac{dp}{dx}+R_\mu u_{yy}, \quad \eta\le y\le h. \tag{4b}$$

Clearly, unless $\mathrm{Re}=\mathrm{O}(\varepsilon^{-2})$ or higher, inertia is negligible. For most lubrication flow problems one expects Re to remain of O(1) or smaller given the heavily viscous fluids used. In this case, inertia is of $\mathrm{O}(\varepsilon^2)$ or smaller and will therefore be neglected in this work. Consequently, Eqs. (4a) and (4b) reduce, respectively, to

$$u_{yy}(x,0\le y\le \eta)=p_x, \tag{5a}$$

$$u_{yy}(x,\eta\le y\le h)=\frac{p_x}{R_\mu}. \tag{5b}$$

Equation (5) must be integrated subject to the no-slip conditions at the rigid boundaries

$$u(x,y=0)=1, \quad u(x,y=h)=0, \tag{6}$$

and the continuity of flow and traction at the interface:

$$u(x,y=\eta^-)=u(x,y=\eta^+), \tag{7a}$$

$$u_y(x,y=\eta^-)=R_\mu u_y(x,y=\eta^+), \tag{7b}$$

where η^- and η^+ are positions just below and just above the interface, respectively. Note that given the absence of inertial and elongational terms, no partial derivatives of u with

respect to x appear. Consequently, there is no need to impose any boundary conditions on u at $x=0$ or $x=1$. On the other hand, boundary conditions are required on the pressure, which will be specified shortly.

Upon noting that the pressure only depends on x, the streamwise velocity component, u, across each fluid layer, is obtained by integrating Eqs. (5a) and (5b), and using conditions (6) and (7), to give

$$u(x,0 \le y \le \eta) = \frac{1}{2}\frac{dp}{dx}y^2 + \frac{[(2\eta - 2h - R_\mu \eta)\eta - R_\mu^2(\eta - h)^2]\frac{dp}{dx} - 2R_\mu}{2(R_\mu \eta - \eta + h)}y + 1, \tag{8a}$$

$$u(x,\eta \le y \le h) = \frac{Rp_x}{2}(y^2 - h^2) + \{[\eta^2(1 - 2R^2 + R) - Rh^2]p_x - 2\}\frac{(y-h)}{2(R\eta - \eta + h)}. \tag{8b}$$

The interface height is dictated by the kinematic condition

$$v(x, y = \eta) = u(x, y = \eta)\eta_x, \tag{9}$$

where $v(x,y)$ is next determined at $y=\eta$ upon integrating the continuity Eq. (3) over the interval $y \in [0, \eta]$ and using expression (8a). In this case, the kinematic condition takes the following form:

$$\frac{d}{dx}\left[\frac{dp}{dx}\eta^3 + 3\left(A\frac{dp}{dx} + B\right)\eta^2 + 6\eta\right] = 0, \tag{10}$$

where $A(\eta,h) = \frac{(2\eta - 2h - R_\mu\eta)\eta - R_\mu^2(\eta-h)^2}{2(R_\mu\eta - \eta + h)}$ and $B(\eta,h) = -\frac{R_\mu}{R_\mu\eta - \eta + h}$. A second relation can be obtained between the volume flux across the channel, Q, and the pressure gradient, namely,

$$\frac{dp}{dx} = \frac{6}{C(\eta,h)}[(1 - R_\mu)(\eta - 2Q)\eta - h^2 + 2Qh], \tag{11}$$

where

$$C(\eta,h) = (R_\mu - 1)^2\eta^4 - 2(3R_\mu^2 - 2R_\mu - 1)h\eta^3 + (9R_\mu^2 - 6R_\mu - 3)h^2\eta^2 - 4R_\mu(R_\mu - 1)h^3\eta - R_\mu h^4.$$

The boundary conditions relevant to the problem are obtained by specifying the level of the interface at inception and noting that the pressure must vanish at the two ends of the flow domain. Thus,

$$\eta(x = 0) = 1, \tag{12a}$$

$$p(x = 0) = p(x = 1) = 0. \tag{12b}$$

An expression for Q is obtained implicitly in terms of η upon integrating Eq. (11) between 0 and 1 and applying the two conditions on pressure from Eq. (11). Hence,

$$Q = \frac{1}{2}\int_0^1 \frac{[(R_\mu - 1)\eta^2 + h^2]dx}{C(h,\eta)} \Bigg/ \int_0^1 \frac{[(R_\mu - 1)\eta + h]dx}{C(h,\eta)}. \tag{13}$$

Once the pressure gradient, interface height, and flow rate are obtained, the streamwise and depthwise velocity components can also be determined. This is detailed next.

B. Solution procedure

Two solution alternatives to obtain p, η, and Q from Eqs. (10), (11), (12a), (12b), and (13) are worth discussing here. The first method consists of eliminating the pressure gradient between Eqs. (10) and (11) and substituting for Q from Eq. (13) to obtain an integral equation for η, which can be solved subject to the first condition in Eq. (12). This can be done by first integrating Eq. (10) to give

$$\eta^2(\eta + 3A)\frac{dp}{dx} + 3B\eta^2 + 6\eta = (1 + 3A_0)\frac{dp_0}{dx} + 3B_0 + 6, \tag{14}$$

where $A_0 = A(\eta = 1, h = R_H)$ and $B_0 = B(\eta = 1, h = R_H)$. Also $\frac{dp_0}{dx} = \frac{dp}{dx}(\eta = 1, h = R_H)$ from Eq. (9). Next, the pressure gradient is eliminated between Eqs. (11) and (14), and Q is substituted from Eq. (13) to finally lead to an integral equation for η, namely,

$$\int_0^1 \frac{[(R_\mu - 1)\eta^2 + h^2]dx}{C(h,\eta)} = D(\eta,h)\int_0^1 \frac{[(R_\mu - 1)\eta + h]dx}{C(h,\eta)}, \tag{15}$$

where

$$D(\eta,h) = \frac{(R_\mu - 1)\eta^2 + h^2 + \left[(1 + 3A_0)\frac{dp_0}{dx} + 3(B_0 - B\eta^2) + 6(1 - \eta)\right]\frac{C(\eta,h)}{6\eta^2(\eta + 3A)}}{R_\mu\eta - \eta + h}.$$

Given the strong nonlinearity involved in Eq. (15), an iterative process must imminently be used. In this case, a good initial guess is required for the solution to converge.

The second approach, which is the one adopted here, consists of setting up the problem as a differential system. Upon carrying out the differentiation in Eq. (10), and eliminating the pressure gradient using Eq. (11), the following equation is obtained for the interface height:

$$\frac{d\eta}{dx} = \frac{E(\eta,h,Q)}{F(\eta,h,Q)}, \tag{16}$$

where

$$E(\eta,h,Q) = 2\eta^2[(\eta+3A)C_h - 3CA_h] \times[(1-R_\mu)(\eta-2Q)\eta - h^2 + 2Qh] - C\eta^2[B_h - 4(\eta+3A)(Q-h)],$$

and

$$F(\eta,h,Q) = 2[6AC\eta + 3C(1+A_\eta)\eta^2 - \eta^2(\eta+3A)C_\mu] \times[(1-R_\mu)(\eta-2Q)\eta - h^2 + 2Qh] + 4(R_\mu-1)C(\eta+3A)(Q-\eta)\eta^2 + 2BC\eta + B_\eta C\eta^2 + 2.$$

Since Q is still unknown, Eq. (16) cannot be solved separately. In addition, the existence of only one boundary condition on η, Eq. (12a), and two conditions on the pressure, Eq. (12b), forces the problem to be solved as a coupled system. Thus, Eqs. (11) and (16) are solved together subject to conditions (12). The third boundary condition allows the determination of Q. A variety of solution methods can be applied to solve the (eigenvalue) problem as an initial-value problem. Similar problems emerge in other physical systems involving moving boundaries, such as fiber spinning [17,18] and film casting. [15,16] Gelder [17] solved the problem by using a finite-difference approximation, while Fisher and Denn [18] applied a Runge-Kutta method, combined with a shooting technique. In the current study, however, the problem is solved as a two-point boundary-value problem. [16] In this case, Q is regarded as a third dependent variable, although it is a constant.

In summary, the equations to be solved are Eqs. (11) and (16), subject to conditions (12). The resulting two-point boundary-value problem reads

$$\frac{d\eta}{dx} = \frac{E(\eta,h,Q)}{F(\eta,h,Q)},$$

$$\frac{dp}{dx} = \frac{6[(1-R_\mu)(\eta-2Q)\eta - h^2 + 2Qh]}{C(\eta,h)}, \quad \frac{dQ}{dx} = 0, \tag{17a}$$

$$\eta(x=0) = 1, \quad p(x=0) = p(x=1) = 0. \tag{17b}$$

Problem (17) is solved using a variable-order, variable-step size finite-difference scheme with deferred corrections. The basic discretization is the trapezoidal rule over a nonuniform mesh. The mesh is chosen adaptively, to make the local error approximately the same size everywhere. Higher-order discretization is obtained by deferred corrections. Global error estimates are produced to control the computation. The resulting nonlinear algebraic system is solved using Newton's method with step control. The linearized system of equations is resolved by a special form of Gauss elimination that preserves sparseness.

III. DISCUSSION AND RESULTS

The discussion will focus on the influence of viscosity ratio and channel topography. The two fluid layers are assumed to have the same thickness at the entrance to the channel so that $R_H=2$. Two flow configurations of the Reynolds bearing type will be examined, both involving a straight moving lower plate and an upper inclined boundary. In the first configuration, the upper plated is straight, and in the second it is spatially modulated with mean height corresponding to the straight case. In both cases, the flow is contracting.

A. Reynolds-bearing flow with straight upper boundary

Consider the two-layer Reynolds-bearing flow, which consists of the two fluids flowing inside in a channel of linearly varying width. The upper plate decreases linearly with x, and the lower plate is straight. In this case, $h(x)=R_H+Sx$, where S is the (negative) slope. Figure 2 displays the interface height and pressure distributions, for the range of viscosity ratio $R_\mu \in [0.1,10]$, $R_H=2$ and $S=-1/3$. The pressure displays a maximum at some location, for any viscosity ratio, which is expected in lubrication flow. The location of the maximum is closer to flow inception ($x=0$) for the stronger pressure profiles. The interface height is always monotonically increasing with x.

The influence of the viscosity ratio on the pressure and interface height is somewhat intricate. Figure 2 indicates that, while $\eta(x)$ decreases monotonically as R_μ increases, $p(x)$ increases, reaching a maximum, then decreases with viscosity ratio. The maximum pressure distribution (not shown, but see Fig. 5) is reached at $R_\mu \approx 0.3$. Thus, two distinct regimes appear to be discernible. The first regime of low viscosity ratios ($R_\mu < 0.3$), corresponding to the pre-maximum range. In this range, the interface exhibits negative concavity. While the pressure increases strongly with R_μ, the interface height decreases significantly, which is reflected in the jump between the curves corresponding to $R_\mu=0.1$ and 0.5. As the maximum in pressure is reached, $\eta(x)$ grows linearly with x and changes concavity as R_μ increases beyond 0.3. Note that the pressure reaches maximum at every x location. The second regime thus corresponds to the post-maximum range of viscosity ratios ($R_\mu > 0.3$), in which both the pressure and interface decrease monotonically with R_μ, to eventually reach, respectively, $p(x)=0$ and $\eta(x)=1$ as $R_\mu \to \infty$. In this case, basic Couette flow is recovered, whereby fluid 1 continues to flow, while layer 2 becomes essentially solid and remains stationary, like a rigid plate. Note that the case $R_\mu=1$ corresponds to a homogeneous (one-layer) lubrication flow, which is recovered by the present calculation.

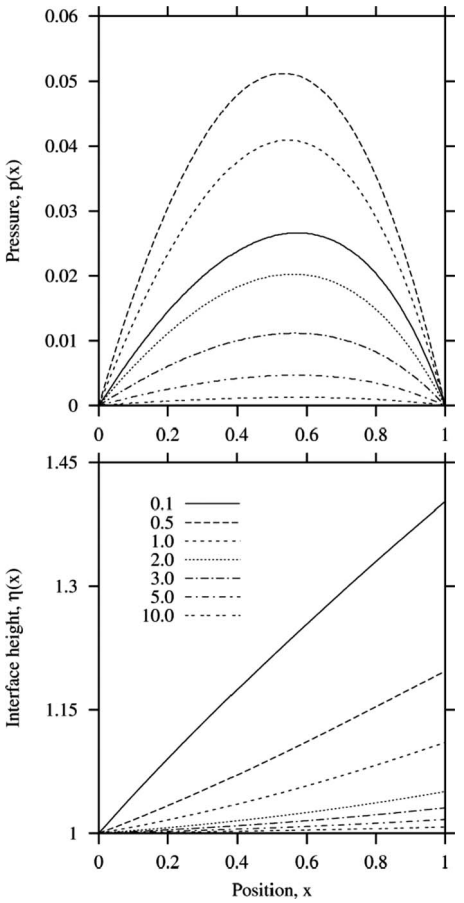

FIG. 2. Influence of viscosity ratio, R_μ, on the interface height, $\eta(x)$, and pressure, $p(x)$, for a linearly contracting channel with lower straight plate. Here $R_\mu \in [0.1, 10]$, $R_H=2$, and $S=-1/3$.

Figure 3 displays the profiles of the horizontal velocity component at different x positions between 0 and 1 for the contracting channel and $R_\mu=0.5$. The velocity tends to display essentially everywhere a Couette character above the interface, linearly decreasing with y, and becoming nonlinear with y below the interface but not changing significantly with x. Another quantity of interest, easily inferable from the profiles in Fig. 3 is the coefficient of friction or shear stress. It is expected that as the flow contracts with x, the shear stress increases. This seems to be indeed the case only at the stationary upper boundary. At the moving flat plate the shear stress decreases with x.

The pressure profiles displayed in Fig. 2 are of course typical of the pressure buildup experienced in lubrication flow. However, this quasiparabolic behavior is not always predicted for any viscosity ratio. Indeed, a significant deviation occurs at very low viscosity ratio. Figure 4 shows the pressure profiles for $R_\mu \in [0.001, 0.1]$. As the viscosity ratio decreases from 0.1, the pressure begins to exhibit an inflexion point, which is located further downstream as R_μ decreases. Moreover, the pressure becomes negative close to the entrance ($x=0$), reflecting a region of expansion relative to the entrance (pool or atmospheric) condition. As R_μ further decreases, the pressure becomes negative everywhere. The interface (not shown) gradually deviates from the linear

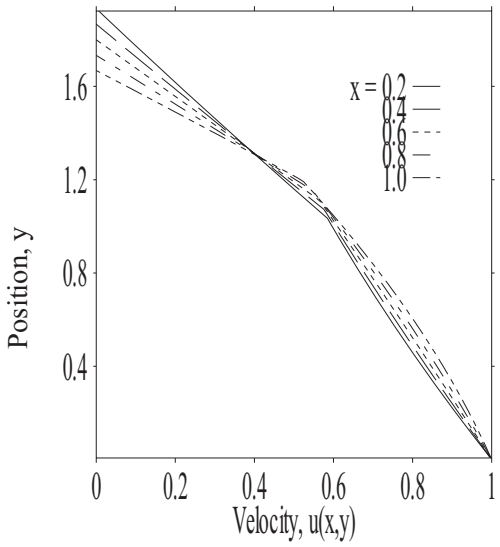

FIG. 3. Horizontal velocity profiles at different x positions for a linearly contracting channel with lower straight plate. Here $R_\mu=0.5$, $x \in [0,1]$, $R_H=2$, and $S=-1/3$.

profile, continually increasing as R_μ decreases. In particular, a sharp gradient develops near the exit. This is the swell effect that is typical of exiting jets.

The pressure buildup with viscosity ratio displayed in Fig. 2 is reminiscent of phase transition and critical phenomena, particularly the case of binary mixtures. [19] The overall picture is further clarified from Fig. 5, which shows the dependence of maximum pressure, $p_{\max}$, its location, $x_{\max}$, and the flow rate, Q, on the viscosity ratio. The pressure maximum increases sharply with R_μ in the low viscosity range, occurring closer to the exit, reaching a maximum, and decreases asymptotically to zero as R_μ tends to infinity. In analogy to binary mixture, the pressure maximum can be compared to the temperature, and the viscosity ratio to the concentration ratio. In this case, the small (high) viscosity range for $p_{\max}$ is comparable to the precritical (postcritical) temperature range. The location, $x_{\max}$, appears to level off for

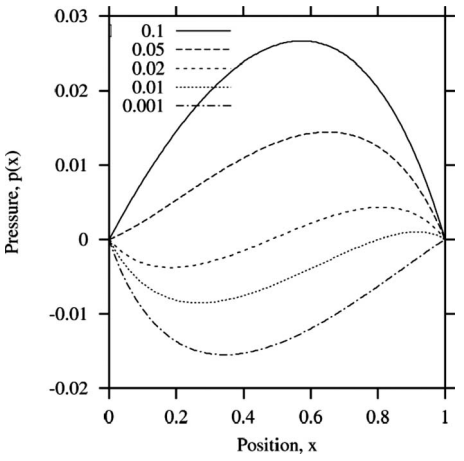

FIG. 4. Pressure distributions in the low-viscosity range for a linearly contracting channel with lower straight plate. Here $R_\mu \in [0.001, 0.1]$, $R_H=2$ and $S=-1/3$.

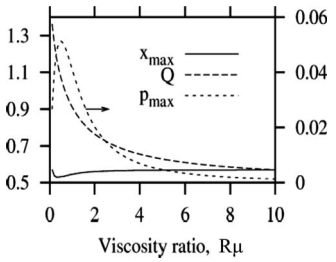

FIG. 5. Dependence of maximum pressure, p_{max}, its location, x_{max}, and the flow rate, Q, on the viscosity ratio for a linearly contracting channel with lower straight plate. Here $R_\mu \in [0.1, 10]$, $R_H=2$, and $S=-1/3$.

$R_\mu > 2$. Similarly to the Gibbs free energy of binary mixtures, x_{max} displays extrema (a strong minimum and a weak maximum). In contrast, the flow rate decreases monotonically with R_μ (rather sharply at small R_μ), and reaches the value of 0.5 at large R_μ, which corresponds to the Couette flow of one-fluid layer through a unit gap. It is interesting to finally observe from Fig. 5 that there exists an optimal viscosity ratio, which is less than one (approximately 0.3), which gives a maximum pressure buildup. This result is of course of important relevance to lubrication flow.

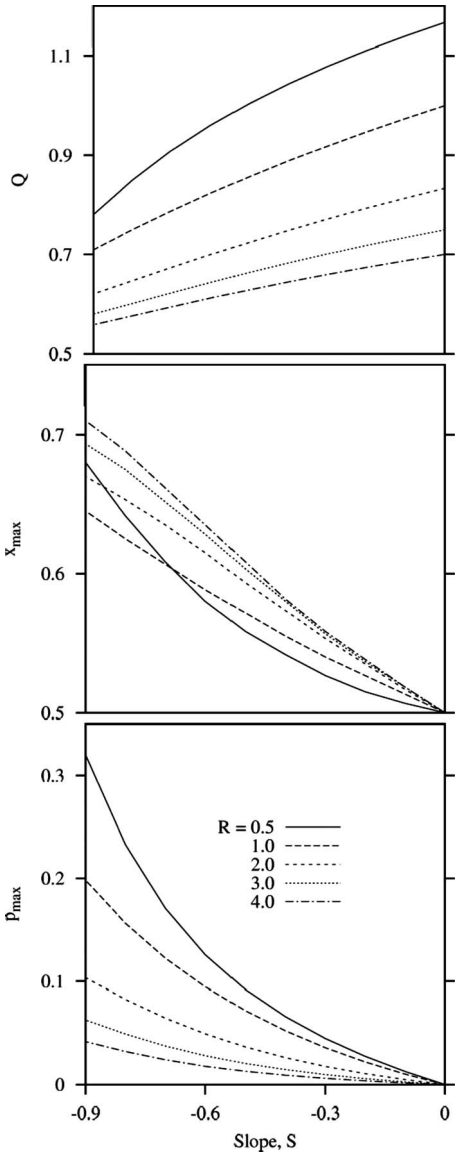

FIG. 6. Dependence of maximum pressure, p_{max}, its location, x_{max}, and the flow rate, Q, on the slope for a linearly contracting channel with lower straight plate. Here $R_\mu \in [0.1, 10]$ and $R_H=2$.

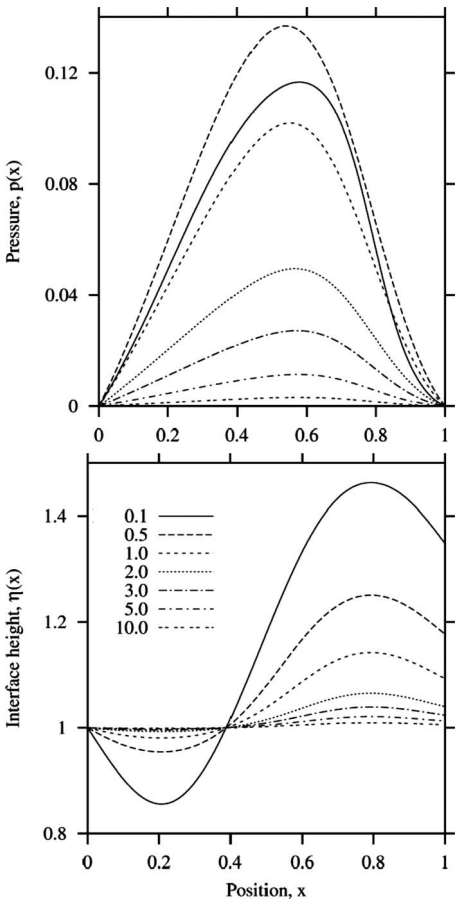

FIG. 7. Influence of viscosity ratio, R_μ, on the interface height, $\eta(x)$, and pressure, $p(x)$, for a linearly contracting and modulated channel with lower straight plate. Here $R_\mu \in [0.1, 10]$, $R_H=2$, $S=-1/3$, $A=0.2$, and $\omega=1$.

The influence of the slope, S, of inclination of the upper plate is illustrated in Fig. 6 for $R_\mu \in [0.5, 4]$. In this range of viscosity ratio, both p_{max} and Q decrease monotonically with R_μ. Generally, and as expected, p_{max} increases sharply with inclination, while Q decreases. However, at large R_μ, the behavior of the pressure, and particularly that of the flow rate, is linear with R_μ. The location of the maximum in pressure, x_{max}, is generally further downstream for higher inclination.

B. Modulated Reynolds-bearing flow

Consider next the flow when the upper boundary is spatially modulated in addition to being inclined, such that $h(x)=R_H+Sx+A\sin(2\pi\omega x)$, where A and ω are the modulation amplitude and wave number. The flow response is typically illustrated in Fig. 7, where $p(x)$ and $\eta(x)$ are plotted for

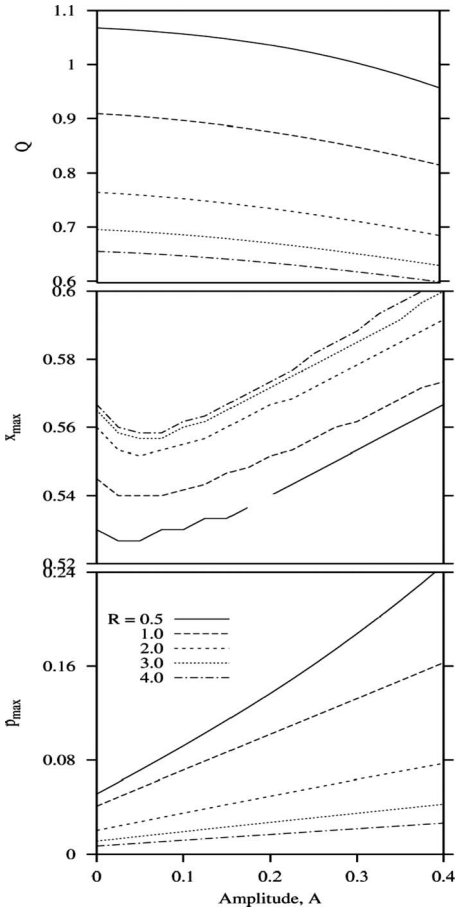

FIG. 8. Dependence of maximum pressure, $p_{\max}$, its location, $x_{\max}$, and the flow rate, Q, on modulation amplitude for a linearly contracting and modulated channel with lower straight plate. Here $R_\mu \in [0.5,4]$, $R_H=2$, $S=-1/3$, and $\omega=0.2$.

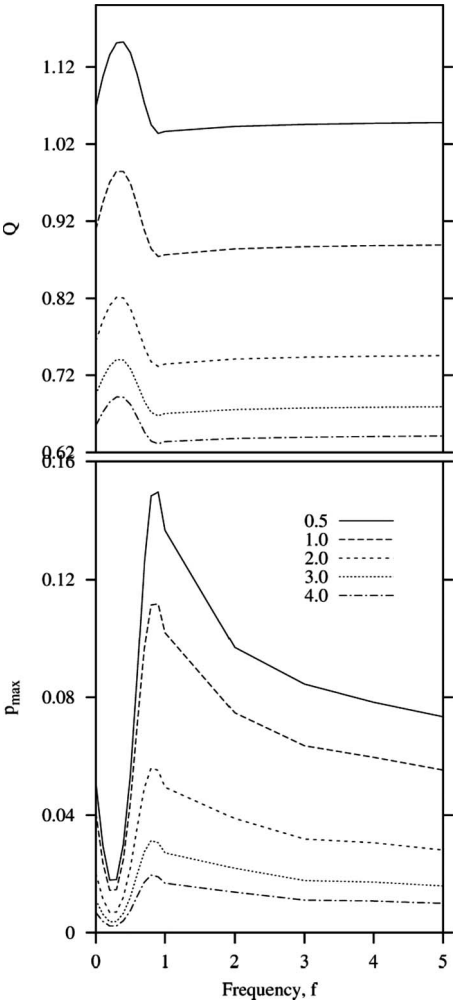

FIG. 9. Dependence of maximum pressure, $p_{\max}$, its location, $x_{\max}$, and the flow rate, Q, on modulation frequency for a linearly contracting and modulated channel with lower straight plate. Here $R_\mu \in [0.5,4]$, $R_H=2$, $S=-1/3$ $A=1$.

$R_H=2$, $S=-1/3$, $A=0.2$ and $\omega=1$. The interface adopts a profile that is out of phase with the boundary modulation. In other words, the interface is higher (lower) where the channel contracts (expands). Interestingly, there is a knot ($\eta=1$), which occurs at the same location ($x\approx 0.4$) regardless of the viscosity ratio, and does not coincide with a pressure extremum. In contrast to the interface height, the pressure is little affected by the modulation, at least qualitatively. Comparison between Figs. 7 and 2 indicates, however, that the pressure buildup has more than doubled as a result of the modulation. In addition, the location of the pressure maximum does not appears to follow a definite trend when R_μ is varied, in contrast to the case when modulation is absent.

Further assessment of the influence of modulation is drawn from Figs. 8 and 9, where $p_{\max}$, $x_{\max}$ and Q are plotted against A and ω, respectively, for $R_\mu \in [0.5,4]$. Generally, the maximum in pressure appears to increase linearly with A, except at small viscosity ratio ($R_\mu < 1$), where the increase is faster for large A. The location of the pressure maximum decreases with A, reaching a minimum, and increases monotonically thereafter. The flow rate decreases monotonically with A. Figure 8 thus indicates that the modulation amplitude tends to prohibit flow causing pressure buildup. Consider finally the influence of ω, which is inferred from Fig. 9 for $A=0.2$. The maximum in pressure appears to experience a minimax behavior as the wave number varies, whereas the flow rate exhibits only a localized maximum. The effect of modulation appears to subside in the limits of small and large wave numbers.

IV. CONCLUDING REMARKS

The planar lubrication flow of two-layer film is examined theoretically in this study. The conservation equations are integrated across each layer, and the problem is reduced to a coupled nonlinear ordinary differential system of the two-point boundary-value type for the pressure, interface height, and flow rate. The flows inside contracting straight and corrugated channels are investigated. The flow is assumed to be induced by the translation of the lower flat plate.

For contracting flow, it is found that two regimes exist as far as the influence of the viscosity ratio, R_μ, is concerned. In particular, the shape of the interface and pressure buildup are determined. In the low R_μ range, the pressure increases with viscosity ratio, everywhere in the flow domain to reach a

maximum at some R_μ. As R_μ increases further the pressure decreases from its maximum level. For spatially modulated channel (around a mean inclined plate), the pressure behaves nonmonotonically with respect to the amplitude and wave number of channel modulation. Considerable pressure buildup and decrease in flow rate are predicted as a result of modulation alone. While the interface exhibits a modulation that is out of phase with boundary modulation, the pressure remains qualitatively unchanged.

The current formulation and solution methodology constitute a general and reliable framework for the modeling of two-layer lubrication flow. Other flow configurations, including other geometries and fluid parameters, are easily tackled, of relevance not only to lubrication flows in mechanical systems but also to physiological systems. The focus in this work is deliberately placed on the pressure distribution and its dependence on viscosity ratio. The primary objective of a lubricant is to keep the two rigid boundaries from coming in contact with one another. This is achieved through the action of the normal force, which consists essentially entirely of a pressure component since other normal stress contributions are essentially absent given the predominantly shearing character of lubrication flow. In this regard, another quantity of interest is the friction coefficient, which is easily determined or even inferred from the velocity profiles as in Fig. 3. The current results clearly show the sensitivity of the pressure to viscosity ratio variation. This can be of direct relevance, for instance, to two-layer lubrication in human synovial joints, where the mechanism of the carrying load is found to be very sensitive to the ratio of layer properties. [20] Understanding the interdependence of the normal and tangential force components is clearly crucial to the design of an effective lubrication process. The addition of another layer seems to alter significantly the flow behavior. Figure 3 shows, for instance, that the friction coefficient increases with position x at the upper stationary boundary, but, in contrast to one-layer film flow, decreases with x at the moving lower plate. Thus, the "wear and tear" or erosion will not happen uniformly at the two boundaries.

[1] I. L. Kliakhandler and G. I. Sivashinsky, Phys. Fluids **9**, 23 (1997).
[2] F. Charru and J. Hinch, J. Fluid Mech. **414**, 195 (2000).
[3] C. Pozrikidis, J. Fluid Mech. **351**, 139 (1997).
[4] C. Pozrikidis, J. Fluid Mech. **371**, 345 (1998).
[5] K. Chen, Phys. Fluids **A5**, 3038 (1993).
[6] D. Dowson, Int. J. Mech. Sci. **4**, 159 (1962).
[7] B. J. Hamrock and D. Dowson, J. Lubr. Technol. **98**, 223 (1976).
[8] K. H. Kim and F. Sadeghi, J. Tribol. **113**, 703 (1991).
[9] T. F. Conry, S. Wang, and C. Cusano, J. Tribol. **109**, 648 (1987).
[10] M. W. Johnson and S. Mangkoesoebroto, J. Tribol. **115**, 71 (1993).
[11] S. Wade, Bull. JSME **20**, 11 (1977).
[12] H. Zhou, R. E. Khayat, R. J. Martinuzzi, and A. G. Straatman, Int. J. Numer. Methods Fluids **39**, 1139 (2002).
[13] M. R. Siddique and R. E. Khayat, Phys. Fluids **14**, 1703 (2002).
[14] K. Alba, R. E. Khayat, and R. S. Pandher, Phys. Rev. E **77**, 056304 (2008).
[15] Y. L. Yeow, J. Fluid Mech. **66**, 613 (1974).
[16] F. Cao, R. E. Khayat, and J. E. Puskas, Int. J. Solids Struct. **42**, 5734 (2005).
[17] D. Gelder, Ind. Eng. Chem. Fundam. **10**, 534 (1971).
[18] R. J. Fisher and M. M. Denn, Chem. Eng. Sci. **30**, 1129 (1975).
[19] L. E. Reichl, *A Modern Course in Statistical Physics* (University of Texas Press, Austin, Texas, 1980).
[20] U. Dinnar, Ann. Biomed. Eng. **4**, 91 (1976).